ADVANCED ELECTRONIC MATERIALS Open Access
www.advelectronicmat.de

Reliable Accessibility of Intermediate Polarization States in Textured Ferroelectric $Al_{0.66}Sc_{0.34}N$ Thin Film

*Tae Yoon Lee, Myeong Seop Song, Jung Woo Cho, In Hyeok Choi, Chihwan An, Jong Seok Lee, and Seung Chul Chae**

Ferroelectric materials are promising candidates for neuromorphic computing synaptic devices due to the nonvolatile multiplicity of spontaneous polarization. To ensure a sufficient memory window, ferroelectric materials with a large coercivity are urgently required for practical applications in highly scaled multi-bit memory devices. Herein, a remarkable reliability of intermediate ferroelectric polarization states is demonstrated in a textured $Al_{0.66}Sc_{0.34}N$ thin film with a coercive field of 2.4 MV cm^{-1}. $Al_{0.66}Sc_{0.34}N$ thin films are prepared at 300 °C on Pt (111)/Ti/SiO_2/Si substrates using a radio frequency reactive sputtering method. $Al_{0.66}Sc_{0.34}N$ thin films exhibit viable ferroelectricity with a large remanent polarization value of >100 μC cm^{-2}. Through the conventional current–voltage characteristics, polarization switching kinetics, and temperature dependence of coercivity, the reproducibility of multiple polarization states with apparent accuracy is attributed to a small critical volume (3.7×10^{-28} m^3) and a large activation energy (3.3×10^{27} eV m^{-3}) for nucleation of the ferroelectric domain. This study demonstrates the potential of ferroelectric $Al_{1-x}Sc_xN$ for synaptic weight elements in neural network hardware.

1. Introduction

The demand for neuromorphic devices has dramatically increased according to rapid developments in artificial intelligence applications.[1–4] In light of the emergence of data-centric processing rather than arithmetic-logic-centric processing for next-generation device applications, not only the traditional memory device architecture but also analog devices for neuromorphic applications have been studied with many order parameters spanning from resistive switching materials to ferroelectrics.[5–11] Among these candidates, the ferroelectric spontaneous polarization has been considered a promising candidate for the robust thermal stability and reproducibility of the analog device.[5] Synaptic devices based on ferroelectrics were demonstrated in the form of a metal-ferroelectric-metal, ferroelectric tunnel junction, and ferroelectric field effect transistor using various ferroelectric materials, such as Pb(Zr, Ti)O_3 (PZT), $BaTiO_3$, and HfO_2.[6–8] Owing to its compatibility with the complementary metal oxide semiconductor process and scalability in the ultimate thickness limit of ferroelectricity, ferroelectric HfO_2 has attracted particular interest.[12,13] Nevertheless, the development of new materials with higher yet viable remanent polarization (P_r) and coercive field (E_c) for the current electronic device operation scheme is essential to improve the resolution of multilevel memory devices and ensure the memory window.[14,15]

The ferroelectric $Al_{1-x}Sc_xN$ has attracted attention with the emergence of switchable ferroelectric polarization under a possible electric stimulus for industrial application.[16] Due to its superior thermal stability and high mechanical quality factor, the wurtzite AlN or $Al_{1-x}Sc_xN$ has been investigated as a piezoelectric and optoelectronic material.[17,18] Recently, Fitchner et al. demonstrated ferroelectricity in $Al_{1-x}Sc_xN$ under a viable operation scheme with a P_r value of 100 μC cm^{-2} and an E_c value of 2–5 MV cm^{-1}.[19] Extensive research revealed that the Sc in $Al_{1-x}Sc_xN$ can cause the flattening of the ionic potential toward the metastable hexagonal structure with a decrease in the aspect ratio of the lattice constant, i.e., the c/a value.[20–22] The Sc doping, therefore, can induce the reduction of coercivity below the dielectric breakdown field. In addition, the alternative modulation of the coercivity of $Al_{1-x}Sc_xN$ was reported through mechanical strain engineering without compositional variation.[23,24] However, Yazawa et al.[25] argued that the modulation of coercivity in ferroelectric $Al_{1-x}Sc_xN$ could be attributed to the Sc content ratio, not the c/a ratio through the detailed crystallographic analysis using X-ray diffraction (XRD). The origin and mechanism of ferroelectricity in wurtzite nitrides remains a topic of controversy. Elucidation of the underlying physics governing the ferroelectric

T. Y. Lee, M. S. Song, J. W. Cho, C. An, S. C. Chae
Department of Physics Education
Seoul National University
Seoul 08826, Republic of Korea
E-mail: scchae@snu.ac.kr
I. H. Choi, J. S. Lee
Department of Physics and Photon Science
Gwangju Institute of Science and Technology (GIST)
Gwangju 61005, Republic of Korea

The ORCID identification number(s) for the author(s) of this article can be found under https://doi.org/10.1002/aelm.202300591

DOI: 10.1002/aelm.202300591

properties of $Al_{1-x}Sc_xN$ is highly needed prior to the ferroelectric device application.

The stability of intermediate partial polarization in ferroelectrics is of interest for the ferroelectric switching dynamics and the critical parameters for the multiplicity of the analog-memory architecture. Analog device development requires an understanding of the stability and reproducibility of intermediate states.[14] The study of the kinetics of ferroelectric polarization switching reveals not only the underlying mechanism of domain growth but also the types and roles of defects involved in polarization reversal.[26,27] For example, due to the presence of dipole defects, ferroelectric polycrystalline PZT films exhibit nucleation-limited ferroelectric switching (NLS) with Lorentzian distribution for the characteristic switching time.[28] In addition, the change of the characteristic switching time under the repeated external electric stimulus, known as the wake-up process revealed that the gradual increase of P_r is attributed to the annihilation of a localized built-in field.[29] In this study, we examined the dynamics of polarization switching and the reproducibility of intermediate polarization states in ferroelectric $Al_{0.66}Sc_{0.34}N$ and its underlying physical causes.

2. Results and Discussion

A textured $Al_{0.66}Sc_{0.34}N$ thin film of the wurtzite structure was grown on a Pt (111)/Ti/SiO_2/Si substrate. **Figure 1**a shows the θ–2θ XRD scans of $Al_{0.66}Sc_{0.34}N$ thin films grown on a Pt (111)/Si substrate. The peaks at approximately 36.4° and 40.0° correspond to the wurtzite $Al_{0.66}Sc_{0.34}N$ (002) and Pt (111) reflections, respectively. For samples with various thicknesses ranging from 52 to 120 nm, the XRD patterns of the $Al_{0.66}Sc_{0.34}N$ thin films exhibit (002) reflection of the wurtzite structure without any secondary phases. The thicknesses of the $Al_{0.66}Sc_{0.34}N$ thin films were confirmed through the cross-section scanning electron microscope (SEM) images, as shown in Figure S1 (see details in Section 1, Supporting Information). The highly *c*-axis oriented $Al_{0.66}Sc_{0.34}N$ thin films, however, exhibited random in-plane crystallinity confirmed by the X-ray pole figure for (103) reflection. Figure 1b shows the X-ray pole figure for the (103) peak of the wurtzite $Al_{0.66}Sc_{0.34}N$ thin films on the Pt (111) layer without a six-fold symmetric diffraction pattern. It indicates that these thin films are c-oriented textured structures without any preferential in-plane orientation. The nature of broken inversion symmetry in $Al_{0.66}Sc_{0.34}N$ thin films was confirmed through the second-harmonic generation (SHG) measurements, as shown in Figure S2 (see details in Section 2, Supporting Information).

The textured $Al_{0.66}Sc_{0.34}N$ thin film exhibited ferroelectric behavior along an external electric stimulus. To characterize the ferroelectric polarization switching, the current density versus the applied electric field (*J*–*E*) loops of $Al_{0.66}Sc_{0.34}N$ thin film were measured by using positive-up-negative-down (PUND) electrical measurements for leakage current compensation (see details in Section 3, Supporting Information). The amplitudes of PUND pulses are 31 and −34 V, respectively, where the asymmetry of applied voltage corresponded to the ferroelectric imprint of the as-grown specimen.[30] **Figure 2**a shows the film thickness dependence of the *J*–*E* loop in ferroelectric $Al_{0.66}Sc_{0.34}N$. The ferroelectric polarization switching current increased rapidly as the

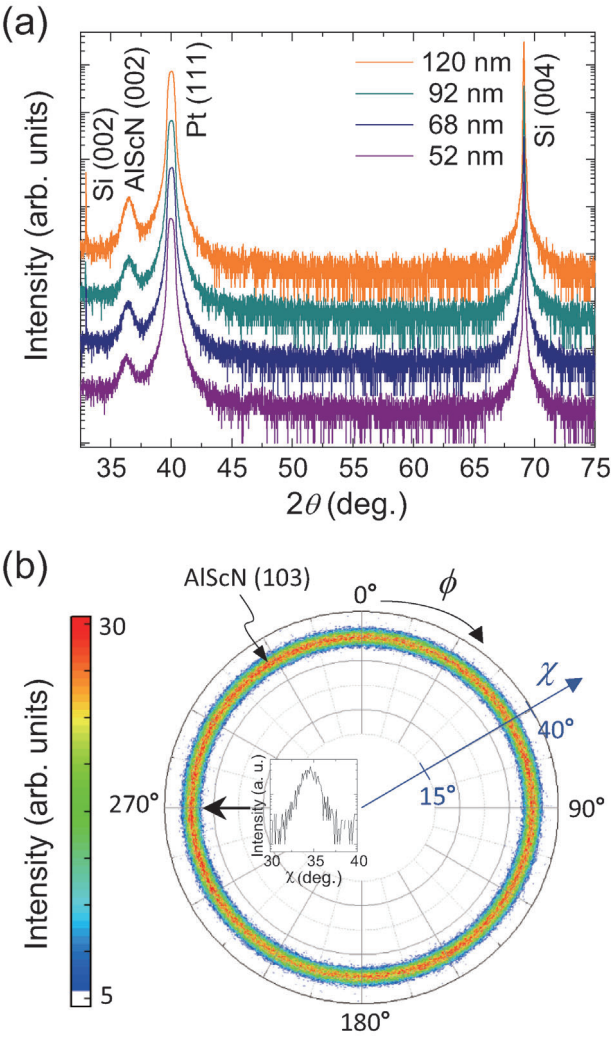

Figure 1. a) X-ray diffraction θ–2θ scan patterns of wurtzite $Al_{0.66}Sc_{0.34}N$ with various film thicknesses ranging from 52 to 120 nm. b) X-ray pole figure of $Al_{0.66}Sc_{0.34}N$ film with a thickness of 120 nm. The inset shows the XRD χ scan patterns at $\phi = 270°$.

thickness of the thin film increased, indicating the increase in the volume ratio of the ferroelectric phase, which is consistent with the results of the SHG analysis. By the integration of ferroelectric polarization switching current, we estimated the *P*-*E* hysteresis as shown in Figure 2b. The ferroelectric $Al_{0.66}Sc_{0.34}N$ thin film exhibited robust E_c and P_r of 2.42 MV cm^{-1} and >100 μC cm^{-2}, respectively. In addition, the ferroelectric $Al_{0.66}Sc_{0.34}N$ thin films exhibited a feasible endurance of up to 10^3 cycles and P_r retention of over 10^4 s, as shown in Figure S4 (see details in Section 4, Supporting Information).

The intermediate ferroelectric polarization states of the $Al_{0.66}Sc_{0.34}N$ thin film demonstrated reliable reproducibility during repeated writing/erasing processes. Before inducing various intermediate states, the ferroelectric polarization was poled downward by a triangular pulse with the amplitude and width of −34 V and 200 μs, respectively. Subsequently, the ferroelectric polarization was partially switched upward from the negatively poled state by a 1 μs-width square pulse with ampli-

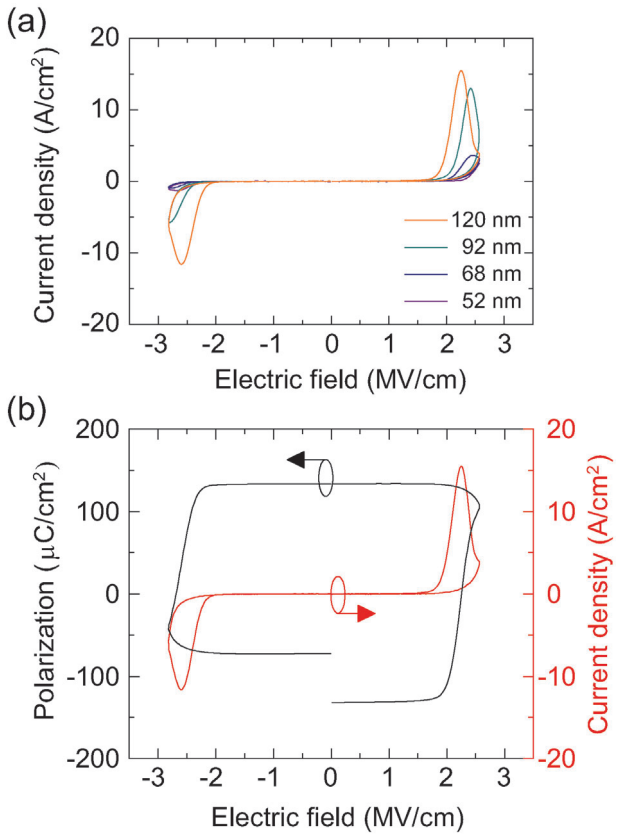

Figure 2. a) Leakage current compensated *J–E* loops of $Al_{0.66}Sc_{0.34}N$ films with different thicknesses measured using a positive-up-negative-down pulse. b) Leakage current compensated *P–E* hysteresis estimated by the integration of ferroelectric polarization switching current in the specimen with a thickness of 120 nm.

tudes varying from 26 to 33 V at 1 V intervals, as shown in Figure S5 (see details in Section 5, Supporting Information). The intermediate ferroelectric polarization states were measured with leakage current compensation. **Figure 3a** shows the inherent multiplicity of $Al_{0.66}Sc_{0.34}N$ ferroelectric polarization states obtained by adjusting the applied pulse voltage from 26 to 33 V. ΔP represents the amount of polarization flipped by an external 1 μs-width square voltage pulse with varying amplitude. As shown in Figure 3b, we obtained a histogram of each subloop state corresponding to $\Delta P/2P_r$ through 30 repeated experiments, where the intermediate states of the ferroelectric $Al_{0.66}Sc_{0.34}N$ films were reproduced with apparent accuracy. All the intermediate polarization state measurements were conducted on an identical single electrode.

The intermediate states of $Al_{0.66}Sc_{0.34}N$ demonstrated high reproducibility for the neuromorphic applications within the statistical acceptance for the practical application. We analyzed the reproducibility of intermediate states through the Weibull analysis by the following equation $F(x) = 1 - \exp[-(\frac{x}{x_0})^k]$, where F(x) is the cumulative probability of a randomly distributed variable ($\Delta P/2P_r$ in this work), and x, x_0, and k are the random variable, scaling constant, and Weibull exponent, respectively. The correlation between k and the ratio of the standard deviation to the mean value in the Weibull distribution is as follows, $\Delta/\mu = \frac{[\Gamma(1+2/k)-\Gamma^2(1+1/k)]^{1/2}}{\Gamma(1+1/k)}$, where Γ represents the Gamma function. In general, the larger the value of k, the higher the reproducibility. As shown in Figure S6 (Supporting Information), the cumulative probabilities of $\Delta P/2P_r$ are well-fitted to the Weibull function. In addition, the cumulative probabilities for various writing pulses are nearly vertical, indicating the reliable reproducibility of the subloop states. Based on the probability distributions of the Weibull function from the fitting results, the margins of absolute error for each subloop state range from 0.8% to 1.3% of the $2P_r$ value with a probability of 99.5% (see details in Section 7, Supporting Information). As illustrated in Figure 3c, as the voltage of the write pulse increased from 26 to 33 V, the value of Δ/μ decreased from 0.0547 to 0.0037 and the value of k increased from 23 to 349. Regarding the reproducibility of previously reported resistive switching materials with the ratio of standard deviation to mean value and the value of k range from ≈0.67 to 0.02 and from 1 to 50, respectively,[9–11] the obtained reproducibility of the intermediate states of $Al_{0.66}Sc_{0.34}N$ demonstrates high feasibility for the neuromorphic application.

The subloop properties of $Al_{0.66}Sc_{0.34}N$ exhibited gradual polarization reversal during the potentiation and depression process with three types of programming pulse trains. Due to their nonvolatile intermediate polarization states, thin ferroelectric films have been considered for synaptic weights.[31] By applying a voltage pulse train with a constant or incremental amplitude and width, it is possible to achieve intermediate polarization states in ferroelectrics.[32] To investigate the synaptic behavior of the ferroelectric $Al_{0.66}Sc_{0.34}N$ thin film, we conducted potentiation and depression experiments using various programming pulse trains.[31,33] As shown in **Figure 4a**, three types of pulse trains commonly used in neuromorphic devices were applied for potentiation and depression, and $\Delta P/2P_r$ values were monitored. Each intermediate state was measured using the 2.5 kHz triangular pulse with amplitudes of −34 and 31 V. As shown in Figure 4b,c, all three pulses were used for long-term potentiation and depression, and analog behavior was observed until the saturation of polarization reversal.

The high linearity of the partial switching of the spontaneous polarization during the potentiation and depression processes was observed using a programming pulse train with gradually increasing amplitudes. The linearity of weight updates during the long-term potentiation and depression process is crucial to the effectiveness and precision of neuromorphic computing.[33,34] The linearity of the weight update can be quantified as follows,[35] $L = \frac{max|\Delta P_P(n)-\Delta P_D(24-n)|}{2P_r}$ for $n = 1$ to 23, where $\Delta P_p(n)$ and $\Delta P_D(n)$ are the amount of flipped ferroelectric polarization following the nth potentiation pulse and nth depression pulse, respectively. As the neuromorphic device exhibits a linear characteristic, the linearity value L converges to zero. As shown in Figure S8 (Supporting Information), the linearity of the potentiation and depression processes is dependent on the programming pulse scheme, with linearities of 0.87, 0.77, and 0.13 for pulse schemes 1, 2, and 3, respectively. Note that the linearity values reported previously for weight update in ferroelectric-based neuromorphic devices

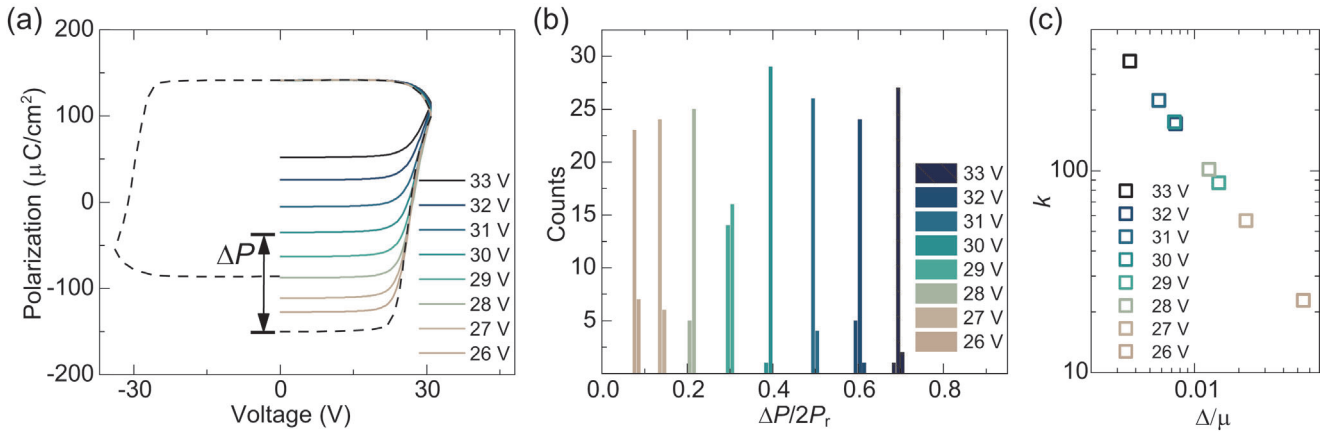

Figure 3. a) Subloop states of $Al_{0.66}Sc_{0.34}N$ using 1 μs-width voltage pulses, b) histogram of each subloop state corresponding to $\Delta P/2P_r$ through 30 repeated experiments, and c) the Weibull slope k versus the standard deviation to the mean ratio of Weibull distribution as a function of the external voltage.

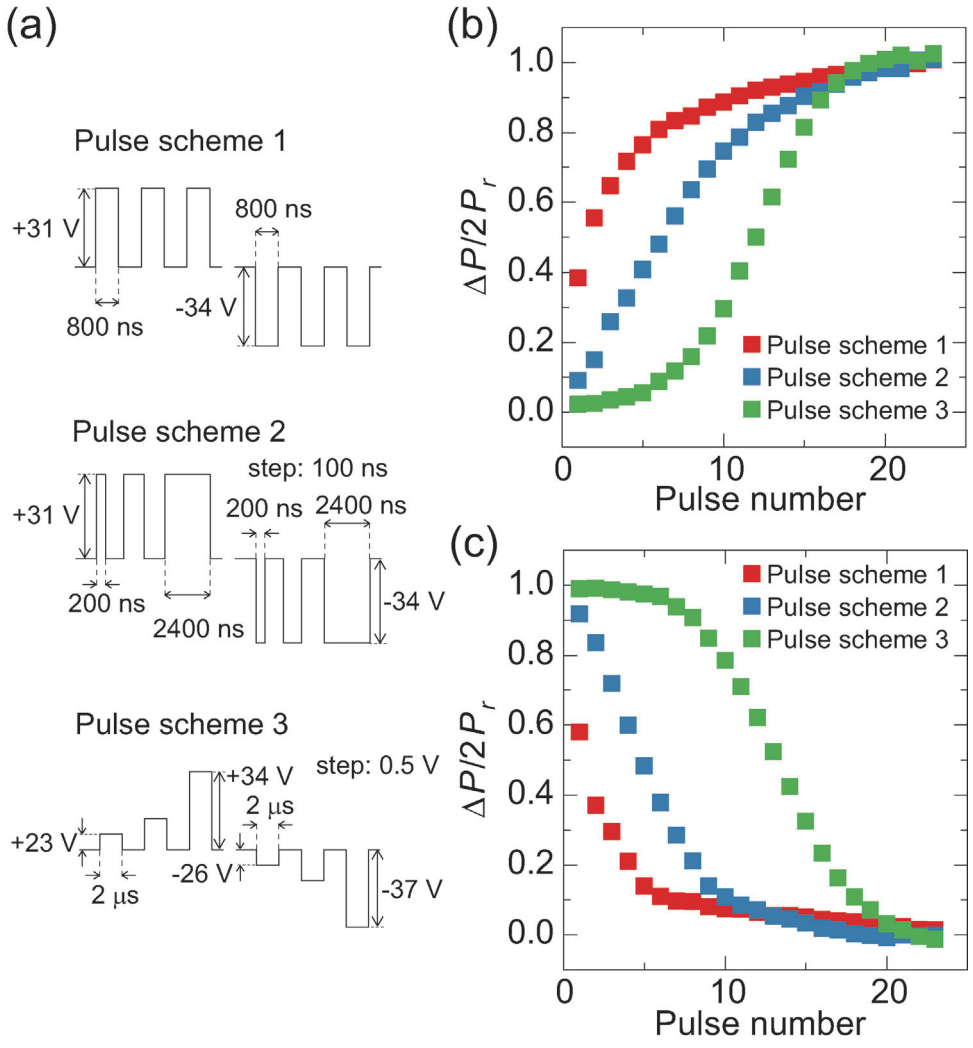

Figure 4. a) Schematic diagrams of the three kinds of programming pulses, b) potentiation, and c) depression behavior of the ferroelectric polarization in the $Al_{0.66}Sc_{0.34}N$ thin film using the three kinds of programming pulses.

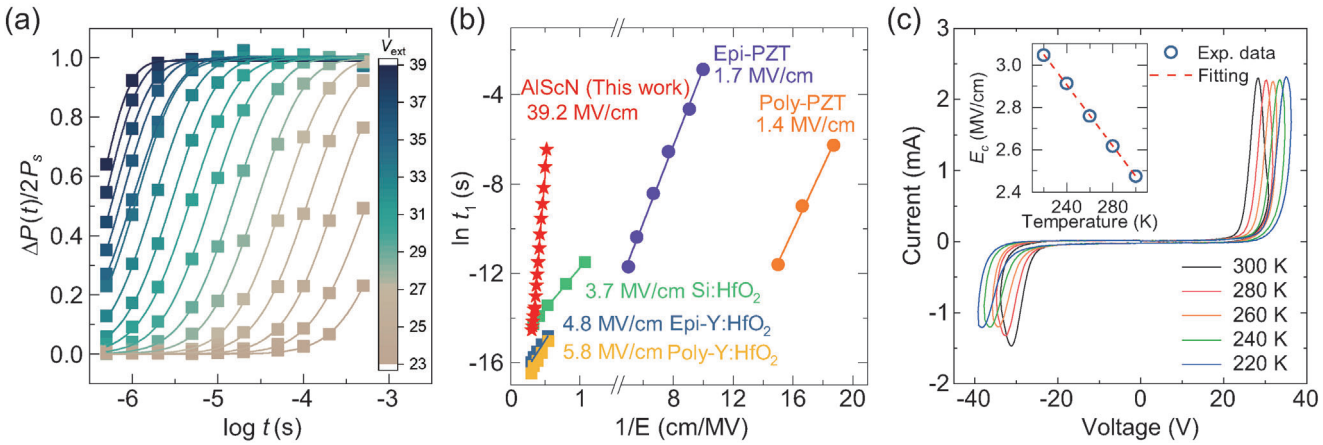

Figure 5. a) Time-dependence of polarization reversal $\Delta P(t)$ as a function of the external voltage V_{ext} at room temperature. b) The external field-dependent characteristic switching time of $Al_{0.66}Sc_{0.34}N$ (this work), typical perovskite and fluorite ferroelectric materials for comparison. Experimental results of epitaxial and polycrystalline PZT, epitaxial and polycrystalline Y doped HfO_2, and polycrystalline Si doped HfO_2 are from Refs. [28] and [43–45]. The solid lines represent fitting results by using Merz's law. c) Temperature dependence of the ferroelectric *I–V* loops. The inset shows the experimental coercive field values at various temperatures and a fitting result obtained using the analytical thermodynamic model.

ranged from 0.25 to 0.6 due to the nonlinearity of ferroelectric polarization switching.[33,35–39]

To elucidate why the ferroelectric $Al_{0.66}Sc_{0.34}N$ exhibited stabilized partial polarization switching behavior, we investigated the detailed switching kinetics of ferroelectric polarization, particularly focusing on the nucleation and domain propagation, using the NLS model. The origin of the characteristic switching time distribution could lie in the inhomogeneities present in the textured polycrystalline films. The grain boundary attributed to the random in-plane crystallinity in *c*-axis oriented textured $Al_{1-x}Sc_xN$ thin films hinders domain wall growth, and its structural disorder can induce the variation of nucleation time of the ferroelectric domain. Recently, there have been some reports on the polarization switching kinetics of $Al_{1-x}Sc_xN$ thin films.[30,40] Yazawa et al.[40] introduced the extended model of nucleation and domain growth, aiming to circumvent the issue of unreasonably large domain growth dimensions as obtained from the analysis using the KAI model. However, our $Al_{0.66}Sc_{0.34}N$ thin film exhibited small values for dimension of the domain growth in the analysis using the KAI model, as shown in Figure S9b (see details in Section 9, Supporting Information). Although analysis using the KAI model is still valid, we believe that analysis using a model with the domain growth dimension value of two and an appropriate distribution of characteristic switching time attributed to the nonuniformity of the specimen has more physical meaning. Thus, due to the inhomogeneous crystallinity and presence of a nonuniform local field in textured $Al_{1-x}Sc_xN$ thin films, the NLS model with a Gaussian distribution for the characteristic switching time was employed to analyze the polarization switching kinetics.[41]

The unprecedentedly large activation field of the ferroelectric $Al_{0.66}Sc_{0.34}N$ has been revealed through analysis of ferroelectric switching dynamics. **Figure 5a** shows the time-dependent switched polarization value as a function of external voltage. All time-dependent switched polarization measurements were conducted on an identical single electrode. Experimental details of time-dependent switched polarization measurement are provided in Section 10, Supporting Information. The solid lines correspond to the fitting results using the NLS model with a Gaussian distribution for the characteristic switching time as follows:[28,41]

$$\frac{\Delta P(t)}{2P_s} = \int_{-\infty}^{\infty} \left[1 - exp\left\{-\left(\frac{t}{t_0}\right)^2\right\}\right] \mathrm{F}(\log t_0)\, d(\log t_0) \qquad (1)$$

where $\mathrm{F}(\log t_0) = \frac{A}{\sigma\sqrt{2\pi}} exp\{-\frac{1}{2}(\frac{\log t_0 - \log t_1}{\sigma})^2\}$. A, σ, and $\log t_1$ are the normalization constant, standard deviation, and mean value of the distribution, respectively. The generic ferroelectric domain reversal in polycrystalline ferroelectric thin films is denoted by the nucleation process and is followed by the propagation of the domain wall with diverse characteristic switching times.[27] Figure 5b shows the $1/E$ dependence of $\ln(t_1)$ obtained from the analysis of the polarization switching kinetics, where scatters and solid lines represent the experimental and the fitting results, respectively. The linear relationship between $1/E$ and $\ln(t_1)$ indicates that the characteristic switching time follows the empirical Merz's law, $t_1 = t_\infty \exp(\frac{E_a}{E})$, where t_∞, E, and E_a are the switching time under an infinite applied electric field, the applied electric field, and the activation field, respectively.[42] In the $Al_{0.66}Sc_{0.34}N$ thin film, as shown in Figure 5b, the activation field calculated using Merz's equation is approximately 39.2 MV cm^{-1}, considerably greater than other ferroelectrics, such as PZT and hafnium-based thin films.[28,43–45]

To understand the robust reproducibility and stability of the intermediate polarization states, we examined the temperature dependence of coercivity in $Al_{0.66}Sc_{0.34}N$. Figure 5c depicts the current versus voltage (*I–V*) loops of $Al_{0.66}Sc_{0.34}N$ thin film measured in 20 K intervals from 220 to 300 K. As shown in the inset of Figure 5c, the temperature-dependent coercivity of $Al_{0.66}Sc_{0.34}N$ thin films exhibited a strong linear behavior along the temperature gradient. E_c is the mean of $|E_{c+}|$ and $|E_{c-}|$. The E_{c+} and E_{c-} values represent the peak position of the switching currents for the upward and downward polarizations, respectively. In the

classical Landau–Devonshire free-energy framework, Vopsaroiu et al. introduce the analytical relationship between temperature and E_c as follows,[46]

$$E_c = \frac{W_B}{P_s} - \frac{k_b T}{V^* P_s} \ln\left(\frac{\nu_0 t}{\ln(2)}\right) \quad (2)$$

where W_B, V^*, P_s, ν_0, k_b, T, and t represent the energy barrier per unit volume, critical volume for nucleation, spontaneous polarization, phonon frequency, Boltzmann constant, temperature, and measurement time, respectively. Based on nonequilibrium statistics of the domain nucleation process, the analytical thermodynamic model has been derived for polarization switching kinetics of second-order phase transition ferroelectrics. This equation can be used to study time and temperature-dependent P–E loops of ferroelectrics, and in particular to investigate the W_B and V^*. For instance, the W_B and V^* of various ferroelectric materials have recently been appraised through this analytical model.[6,47,48] To estimate the W_B and V^* values of $Al_{0.66}Sc_{0.34}N$, we used the phonon frequency and our experimental P_s value (1.81×10^{13} Hz and 113 μC cm^{-2}).[49] The energy barrier per unit volume and critical volume for nucleation were estimated to be 3.3×10^{27} eV m^{-3} and 3.7×10^{-28} m^3, respectively.

The remarkable reliability of the multi-level polarization states in the ferroelectric $Al_{0.66}Sc_{0.34}N$ thin films is attributed to the high energy barrier per unit volume and small critical volume for nucleation. The small critical volume and high energy barrier for nucleation strongly correspond to the robust accessibility to the intermediate state and stability of the intermediate state.[6,47,48] The domain reversal in ferroelectric materials is initiated by independent nucleation, followed by domain-wall propagation under the influence of an external electric field. A fine ferroelectric domain nucleation originating from the small critical volume enables precise control of partial polarization switching.[6] Furthermore, the high energy barrier indicates the difficulty in thermal polarization reversal.[6,47,48] In this context, the high energy barrier (3.3×10^{27} eV m^{-3}) for the nucleation of ferroelectric $Al_{0.66}Sc_{0.34}N$ and small critical volume (3.7×10^{-28} m^3) with respect to conventional perovskite material, for example, PZT[48] are responsible to its high accessibility and stability of intermediate polarization states.

3. Conclusion

In summary, we have investigated the partial switching behavior of the ferroelectric domain in textured $Al_{0.66}Sc_{0.34}N$ thin films. The intermediate polarization states of the $Al_{0.66}Sc_{0.34}N$ exhibited remarkable reliability and reproducibility with apparent accuracy. The NLS model explains the polarization switching kinetics of the $Al_{0.66}Sc_{0.34}N$ where the characteristic switching time exhibits the Gaussian distribution. Furthermore, the external field dependence of the characteristic switching time demonstrated the unprecedentedly large activation field of 39.2 MV cm^{-1} for domain growth. The temperature-dependent coercivity of the $Al_{0.66}Sc_{0.34}N$ reveals the small critical volume and the high energy barrier for the nucleation of ferroelectric domains. The remarkable reliability of multi-level polarization states is attributed to the small critical nucleation volume and high energy barrier of the $Al_{0.66}Sc_{0.34}N$. In addition, the synaptic properties of the $Al_{0.66}Sc_{0.34}N$ exhibited high linearity in the potentiation and depression process. Our results demonstrate the potential of ferroelectric $Al_{1-x}Sc_xN$ for synaptic device applications enabling neuromorphic computing.

4. Experimental Section

Wurtzite $Al_{0.66}Sc_{0.34}N$ thin films were deposited on a Pt (111)/Ti/SiO_2/Si substrate by radio frequency (RF) reactive magnetron sputtering with an $Al_{0.6}Sc_{0.4}$ metal alloy target of 1-inch diameter. The RF power and deposition temperature were maintained at 52 W and 300 °C, respectively, and the sputtering pressure was maintained at 0.85 Pa by introducing a mixture of Ar/N_2 gas in the ratio of 1:2. The thickness and chemical composition of the $Al_{0.66}Sc_{0.34}N$ films were determined using SEM and X-ray photoelectron spectroscopy (XPS). Details of the stoichiometric characterization of specimens using XPS are provided in Section 11, Supporting Information. For structural analysis, conventional θ–2θ scans of XRD measurements were performed using a Bruker D8 discover with Cu Kα radiation ($\lambda = 0.154$ nm). The X-ray pole figure measurement for $Al_{0.66}Sc_{0.34}N$ (103) was conducted to check the in-plane crystallinity. In SHG measurements, an 800 nm pulsed laser beam with 80 MHz repetition (Vitara-T, *Coherent*) illuminates the samples with out-of-plane (P) and in-plane (S) polarization. A second harmonic wave in P- and S- polarization by using a photomultiplier detector (*Hamamatsu*) with a current pre-amplifier (*SRS*) is monitored. To increase the efficiency of the SHG process, the input laser beam was tightly focused on the sample with a beam size of 2 μm by using an objective lens with a power of about 1.5 mW. For electrical measurements, Pt top electrodes with a thickness of 40 nm were deposited at room temperature using electron beam evaporation. Via photolithography, top electrodes were patterned with an area of 120×120 μm^2. All electrical measurements were conducted using a conventional semiconductor parameter analyzer (4200-SCS, Keithley). Square voltage pulses with a rise/fall time of 50 ns were used for partial polarization switching. The sample was cooled down to 220 K with liquid nitrogen for low-temperature measurements.

Supporting Information

Supporting Information is available from the Wiley Online Library or from the author.

Acknowledgements

This work was supported by the Next-generation Intelligence Semiconductor R&D Program (2022M3F3A2A01079710) and the National Research Foundation of Korea (NRF) grant funded by the Korean government (MSIT) (Grants No. 2021R1A2C1094795 and No. 2022R1A2C2007847). Part of this study was performed using the facilities of the IBS Center for Correlated Electron Systems, Seoul National University.

Conflict of Interest

The authors declare no conflict of interest.

Data Availability Statement

The data that support the findings of this study are available from the corresponding author upon reasonable request.

Keywords

AlScN, ferroelectrics, multilevel, neuromorphic devices, thin films

Received: September 1, 2023
Revised: October 19, 2023
Published online: November 27, 2023

[1] K.-H. Kim, S. Oh, M. M. A. Fiagbenu, J. Zheng, P. Musavigharavi, P. Kumar, N. Trainor, A. Aljarb, Y. Wan, H. M. Kim, K. Katti, S. Song, G. Kim, Z. Tang, J.-H. Fu, M. Hakami, V. Tung, J. M. Redwing, E. A. Stach, R. H. Olsson, D. Jariwala, *Nat. Nanotechnol.* **2023**, *18*, 1044.
[2] T. Li, J. Miao, X. Fu, B. Song, B. Cai, X. Ge, X. Zhou, P. Zhou, X. Wang, D. Jariwala, W. Hu, *Nat. Nanotechnol.* **2023**, https://doi.org/10.1038/s41565-023-01446-8.
[3] T. Mikolajick, M. H. Park, L. Begon-Lours, S. Slesazeck, *Adv. Mater.* https://doi.org/10.1002/adma.2022060422206042.
[4] L. Liu, W. Xiong, Y. Liu, K. Chen, Z. Xu, Y. Zhou, J. Han, C. Ye, X. Chen, Z. Song, M. Zhu, *Adv. Electron. Mater.* **2020**, *6*, 1901012.
[5] Z. Zhao, A. Abdelsamie, R. Guo, S. Shi, J. Zhao, W. Lin, K. Sun, J. Wang, J. Wang, X. Yan, J. Chen, *Nano Res.* **2022**, *15*, 2682.
[6] K. Lee, H.-J. Lee, T. Y. Lee, H. H. Lim, M. S. Song, H. K. Yoo, D. I. Suh, J. G. Lee, Z. Zhu, A. Yoon, M. R. MacDonald, X. Lei, K. Park, J. Park, J. H. Lee, S. C. Chae, *ACS Appl. Mater. Interfaces* **2019**, *11*, 38929.
[7] R. Guo, Y. Zhou, L. Wu, Z. Wang, Z. Lim, X. Yan, W. Lin, H. Wang, H. Y. Yoong, S. Chen, T. V. Ariando, J. Wang, G. M. Chow, A. Gruverman, X. Miao, Y. Zhu, J. Chen, *ACS Appl. Mater. Interfaces* **2018**, *10*, 12862.
[8] G. Zhong, M. Zi, C. Ren, Q. Xiao, M. Tang, L. Wei, F. An, S. Xie, J. Wang, X. Zhong, M. Huang, J. Li, *Appl. Phys. Lett.* **2020**, *117*, 092903.
[9] W.-Y. Chang, K.-J. Cheng, J.-M. Tsai, H.-J. Chen, F. Chen, M.-J. Tsai, T.-B. Wu, *Appl. Phys. Lett.* **2009**, *95*, 042104.
[10] B. Gao, H. W. Zhang, S. Yu, B. Sun, L. F. Liu, X. Y. Liu, Y. Wang, R. Q. Han, J. F. Kang, B. Yu, Y. Y. Wang, *Tech. Dig.-Symp. VLSI Technol* **2009**, 30.
[11] B. J. Choi, A. B. K. Chen, X. Yang, I.-W. Chen, *Adv. Mater.* **2011**, *23*, 3847.
[12] S. S. Cheema, N. Shanker, L.-C. Wang, C.-H. Hsu, S.-L. Hsu, Y.-H. Liao, M. San Jose, J. Gomez, W. Chakraborty, W. Li, J.-H. Bae, S. K. Volkman, D. Kwon, Y. Rho, G. Pinelli, R. Rastogi, D. Pipitone, C. Stull, M. Cook, B. Tyrrell, V. A. Stoica, Z. Zhang, J. W. Freeland, C. J. Tassone, A. Mehta, G. Saheli, D. Thompson, D. I. Suh, W.-T. Koo, K.-J. Nam, et al., *Nature* **2022**, *604*, 65.
[13] M. Cervo Sulzbach, H. Tan, S. Estandía, J. Gàzquez, F. Sánchez, I. Fina, J. Fontcuberta, *ACS Appl. Electron. Mater.* **2021**, *3*, 3657.
[14] S. Oh, H. Hwang, I. K. Yoo, *APL Mater.* **2019**, *7*, 091109.
[15] S. K. Ryoo, K. D. Kim, H. W. Park, Y. B. Lee, S. H. Lee, I. S. Lee, S. Byun, D. Shim, J. H. Lee, H. Kim, Y. H. Jang, M. H. Park, C. S. Hwang, *Adv. Electron. Mater.* **2022**, *8*, 2200726.
[16] D. Wang, P. Wang, S. Mondal, M. Hu, D. Wang, Y. Wu, T. Ma, Z. Mi, *Appl. Phys. Lett.* **2023**, *122*, 052101.
[17] C.-M. Lin, T.-T. Yen, V. V. Felmetsger, M. A. Hopcroft, J. H. Kuypers, A. P. Pisano, *Appl. Phys. Lett.* **2010**, *97*, 083501.
[18] L. W. Hung, C. T. C. Nguyen, *J. Microelectromech. Syst.* **2015**, *24*, 458.
[19] S. Fichtner, N. Wolff, F. Lofink, L. Kienle, B. Wagner, *J. Appl. Phys.* **2019**, *125*, 114103.
[20] S. Zhang, D. Holec, W. Y. Fu, C. J. Humphreys, M. A. Moram, *J. Appl. Phys.* **2013**, *114*, 133510.
[21] S. Yasuoka, T. Shimizu, A. Tateyama, M. Uehara, H. Yamada, M. Akiyama, Y. Hiranaga, Y. Cho, H. Funakubo, *J. Appl. Phys.* **2020**, *128*, 114103.
[22] K. Yazawa, A. Zakutayev, G. L. Brennecka, *Appl. Phys. Lett.* **2022**, *121*, 042902.
[23] S. Yasuoka, R. Mizutani, R. Ota, T. Shiraishi, T. Shimizu, M. Uehara, H. Yamada, M. Akiyama, H. Funakubo, *ACS Appl. Electron. Mater.* **2022**, *4*, 5165.
[24] K. Yazawa, D. Drury, A. Zakutayev, G. L. Brennecka, *Appl. Phys. Lett.* **2021**, *118*, 162903.
[25] K. Yazawa, J. S. Mangum, P. Gorai, G. L. Brennecka, A. Zakutayev, *J. Mater. Chem. C* **2022**, *10*, 17557.
[26] Y. Ishibashi, Y. Takagi, *J. Phys. Soc. Jpn.* **1971**, *31*, 506.
[27] A. K. Tagantsev, I. Stolichnov, N. Setter, J. S. Cross, M. Tsukada, *Phys. Rev. B* **2002**, *66*, 214109.
[28] J. Y. Jo, H. S. Han, J. G. Yoon, T. K. Song, S. H. Kim, T. W. Noh, *Phys. Rev. Lett.* **2007**, *99*, 267602.
[29] T. Y. Lee, K. Lee, H. H. Lim, M. S. Song, S. M. Yang, H. K. Yoo, D. I. Suh, Z. Zhu, A. Yoon, M. R. MacDonald, X. Lei, H. Y. Jeong, D. Lee, K. Park, J. Park, S. C. Chae, *ACS Appl. Mater. Interfaces* **2019**, *11*, 3142.
[30] S. Fichtner, F. Lofink, B. Wagner, G. Schönweger, T. N. Kreutzer, A. Petraru, H. Kohlstedt, *2020 Joint Conf. IEEE Int. Frequency Control Symp. Int. Symp. Applications of Ferroelectrics* **2020**, 1.
[31] M.-K. Kim, J.-S. Lee, *Nano Lett.* **2019**, *19*, 2044.
[32] J. Woo, K. Moon, J. Song, M. Kwak, J. Park, H. Hwang, *IEEE Trans. Electron Devices* **2016**, *63*, 5064.
[33] J. Li, C. Ge, J. Du, C. Wang, G. Yang, K. Jin, *Adv. Mater.* **2020**, *32*, 1905764.
[34] R. Islam, H. Li, P.-Y. Chen, W. Wan, H.-Y. Chen, B. Gao, H. Wu, S. Yu, K. Saraswat, H. S. Philip Wong, *J. Phys. D. Appl. Phys.* **2019**, *52*, 113001.
[35] I. T. Wang, C.-C. Chang, L.-W. Chiu, T. Chou, T.-H. Hou, *Nanotechnology* **2016**, *27*, 365204.
[36] S. Majumdar, H. Tan, Q. H. Qin, S. van Dijken, *Adv. Electron. Mater.* **2019**, *5*, 1800795.
[37] S. Choi, S. H. Tan, Z. Li, Y. Kim, C. Choi, P.-Y. Chen, H. Yeon, S. Yu, J. Kim, *Nat. Mater.* **2018**, *17*, 335.
[38] X. Zhu, D. Li, X. Liang, W. D. Lu, *Nat. Mater.* **2019**, *18*, 141.
[39] Y. van de Burgt, E. Lubberman, E. J. Fuller, S. T. Keene, G. C. Faria, S. Agarwal, M. J. Marinella, A. Alec Talin, A. Salleo, *Nat. Mater.* **2017**, *16*, 414.
[40] K. Yazawa, J. Hayden, J.-P. Maria, W. Zhu, S. Trolier-McKinstry, A. Zakutayev, G. L. Brennecka, *Mater. Horiz.* **2023**, *10*, 2936.
[41] Y. A. Genenko, S. Zhukov, S. V. Yampolskii, J. Schütrumpf, R. Dittmer, W. Jo, H. Kungl, M. J. Hoffmann, H. von Seggern, *Adv. Funct. Mater.* **2012**, *22*, 2058.
[42] W. J. Merz, *Phys. Rev* **1954**, *95*, 690.
[43] Y. W. So, D. J. Kim, T. W. Noh, J.-G. Yoon, T. K. Song, *Appl. Phys. Lett.* **2005**, *86*, 092905.
[44] P. Buragohain, A. Erickson, T. Mimura, T. Shimizu, H. Funakubo, A. Gruverman, *Adv. Funct. Mater.* **2022**, *32*, 2108876.
[45] M. C. Chun, S. Park, S. Park, G.-y. Park, M. J. Kim, Y. Cho, B. S. Kang, *J. Alloy. Compd.* **2020**, *823*, 153777.
[46] M. Vopsaroiu, J. Blackburn, M. G. Cain, P. M. Weaver, *Phys. Rev. B* **2010**, *82*, 024109.
[47] D. Zhou, Y. Guan, M. M. Vopson, J. Xu, H. Liang, F. Cao, X. Dong, J. Mueller, T. Schenk, U. Schroeder, *Acta Mater.* **2015**, *99*, 240.
[48] Y. Nomura, T. Tachi, T. Kawae, A. Morimoto, *Phys. Status Solidi B* **2015**, *252*, 833.
[49] D. Solonenko, A. Žukauskaitė, J. Pilz, M. Moridi, S. Risquez, *Micromachines* **2022**, *13*, 1961.